

Antireflection-coated blue GaN laser diodes in an external cavity and Doppler-free indium absorption spectroscopy

Lars Hildebrandt, Richard Knispel, Sandra Stry, Joachim R. Sacher, and Frank Schael

Commercially available GaN-based laser diodes were antireflection coated in our laboratory and operated in an external cavity in a Littrow configuration. A total tuning range of typically 4 nm and an optical output power of up to 30 mW were observed after optimization of the external cavity. The linewidth was measured with a heterodyne technique, and 0.8 MHz at a sweep time of 50 ms was obtained. The mode-hop-free tuning range was more than 50 GHz. We demonstrated the performance of the laser by detecting the saturated absorption spectrum of atomic indium at 410 nm, allowing observation of well-resolved Lamb dips. © 2003 Optical Society of America

OCIS codes: 140.2020, 140.3600, 300.1030, 300.6260.

1. Introduction

Since their advent in 1962,^{1–3} semiconductor lasers have found applications in many optical systems, including bar-code scanners, laser printers, telecommunication systems, compact-disc players, and optical sensors. However, for high-precision atom absorption spectroscopy or gas analysis, wavelength tuning and spectral characteristics of commercially available standard laser diodes (LDs) are often far from ideal.⁴ Common strategies to overcome the limited applicability of standard LDs for spectroscopic experiments include implementation of grating or Bragg reflection structures in LD chips (distributed-feedback and distributed-Bragg-reflection LDs). Operation of standard LDs in an external cavity provides an alternative approach.

Recent improvements in room-temperature diode laser technology for data-storage applications have also given rise to increased availability of GaN-based

semiconductor lasers in the blue spectral region (approximately 395–425 nm), which exhibit emission wavelengths, beam profiles, and duty lifetimes (>10,000 h) that are attractive for spectroscopic experiments.^{5,6} To the best of our knowledge, distributed-feedback structures for GaN LDs are not currently available.

Since the appearance of the first external cavity arrangements in 1964,⁷ a number of external cavity diode laser (ECDL) arrangements have been introduced. Among the most simple arrangements is a design similar to the one described by Ricci *et al.*⁸ In this design, the radiation emitted from an antireflection- (AR-) coated front facet of a LD is collimated and hits a holographic grating under Littrow angle (Littrow ECDL). The light diffracted in the first order is reflected back into the LD, whereas the light diffracted in the zeroth order is coupled out and can be used for the experiments. The wavelength change is achieved by means of tilting the grating. However, tilting the grating results in alteration of the beam output direction. A beam-correction mirror can be applied, but tilting the grating still leads to a parallel shift of the output beam.⁹ A second concept is an external cavity in a grazing-incidence configuration similar to the design from Littman *et al.* (Littman ECDL).¹⁰ Again, the output beam of the LD is directed onto a grating. The first diffraction order of the grating rectangularly hits a reflecting element (mirror or prism) and is reflected back onto the grating. The laser resonator is set up between the back facet of the LD and the reflecting element.

L. Hildebrandt (lars@sacher-laser.com), R. Knispel, S. Stry, and J. R. Sacher are with the Sacher Lasertechnik Group, Hannah Arendt Strasse 3-7, D-35037 Marburg, Germany. When this research was performed, F. Schael was with the Institute of Chemistry, Physical Chemistry, University of Potsdam, Karl-Liebknecht-Strasse 24-25, D-14476 Golm, Germany. His current address is Ehrfeld Mikrotechnik AG, Mikroforum 1, D-55234 Wendelsheim, Germany.

Received 20 May 2002; revised manuscript received 15 July 2002.

0003-6935/03/122110-09\$15.00/0

© 2003 Optical Society of America

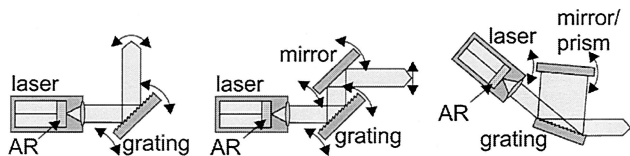


Fig. 1. ECDL in Littrow configuration without (left), with (middle) beam-correction mirror, and in Littman configuration (right).

Wavelength tuning is achieved by means of tilting the reflection element. Figure 1 schematically shows the basic design of the Littrow and Littman ECDL. Both ECDL types contain a mechanically moving part (grating or mirror/prism, respectively) for wavelength tuning. More recently, ECDL concepts without moving parts were described that, for example, employ a liquid-crystal array¹¹ or an electrooptical modulator.^{12,13} Since our first successful AR coating of the GaN-based LD, both Littrow and Littman configurations were proved to work with these diodes.^{14,15} The objective of the current study is to characterize the performance of our Littrow cavity with an implemented AR-coated GaN LD. Doppler-free absorption measurements of indium vapor were performed to show the performance of the laser system at this wavelength. Indium is of particular interest for applications in atom lithography and might also be an interesting new candidate for atom trapping and cooling experiments. For such experiments, laser light from a stable and easy-to-use turnkey laser system with a small linewidth, high output power, and a good side-mode suppression is required.

2. Antireflection Coating of Blue GaN Laser Diodes

Applying high-quality AR coatings to laser diodes is an important processing step before diode lasers are implemented into an external cavity. The quality of the AR coating and the interaction of the LD with the optical feedback critically influences the physical properties of the ECDL. To achieve the lowest reflectivity data, we have used the coating method with *in situ* monitoring of the diode laser.¹⁶ As result of the coating, we achieved a significant change in the threshold current of the diode laser, as seen in Fig. 7, below. We performed an analysis of the optical spectra shown in Fig. 2 for determining the reflectivity of the laser facet.¹⁷ The arrow in Fig. 2 indicates the minimum of the reflectivity. As result of the analysis we find the reflectivity value to be below 1×10^{-5} .

Our goal in this section is to discuss the influence of the performance of AR coating on the physical properties of diode lasers. AR coatings have three different effects on LDs.

A. Emission Direction Effect

AR coating of a diode laser facet changes the symmetric laser emission into a directed emission with

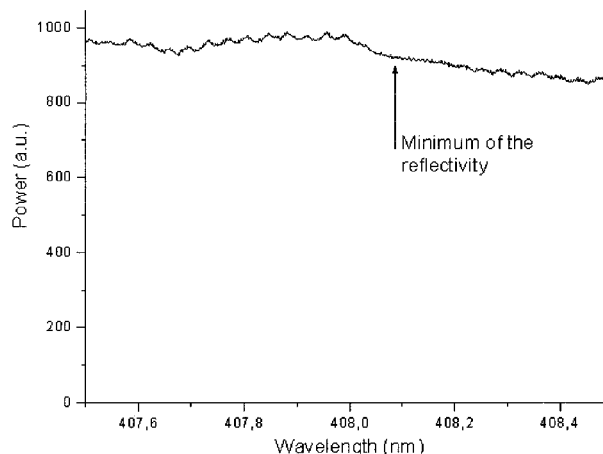
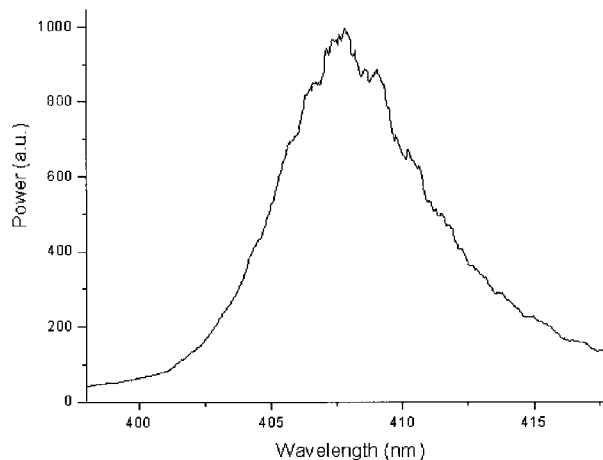


Fig. 2. Optical spectra for describing the performance of the blue GaN diode laser after AR coating. Top, gain width of the GaN diode laser. This curve allows us to give an estimation of the total tuning range. Bottom, optical spectrum measured with a higher resolution in order to determine the reflectivity of the AR-coated laser facet. The arrow indicates the minimum of the reflectivity.

the main emission power from this laser facet. Figure 3 gives an introduction to the formal description of a simplified laser cavity. I_1 is the intensity of the laser light emitted from the facet $x = 0$ with the facet reflectivity R_1 . I_2 is the laser light emitted from the facet $x = L$ with the facet reflectivity R_2 . I_3 is the laser light within the laser cavity that gets amplified during the transition through the laser chip from $x = L$ to $x = 0$. I_4 is the laser light within the laser cavity

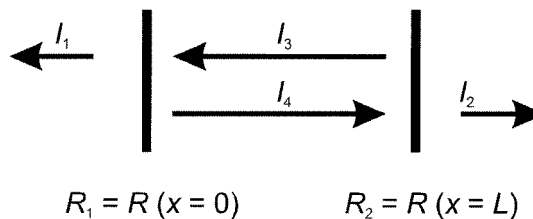


Fig. 3. Schematic drawing of a diode laser cavity.

that gets amplified during the transition through the laser chip from $x = 0$ to $x = L$. As one can see from Fig. 3, the ratio of I_1/I_2 results in

$$\frac{I_1}{I_2} = \frac{1 - R_1}{1 - R_2} \left(\frac{R_2}{R_1} \right)^{1/2}. \quad (1)$$

Equation (1) describes the beam direction effect of AR coatings of diode lasers. One can clearly see the strong effect that a small change in the facet reflectivity has on the emission ratio I_1/I_2 between optical power emitted from the front and the rear facets of the laser.

B. Effect on the Power-Injection Curve

One of the most obvious effects of AR coatings on LDs is the effect on the threshold current and on the quantum efficiency of the LD as seen in Fig. 7 below. For an understanding of this effect one needs to start with the rate equation description of semiconductor LDs as they are given in Ref. 18.

$$\frac{dN}{dt} = J - \frac{N}{\tau_n} - \frac{dg}{dN} (N - N_{th})S, \quad (2)$$

$$\frac{dS}{dt} = \Gamma_{conf} \frac{dg}{dN} (N - N_{th})S - \frac{S}{\tau_s} + \beta \Gamma_{conf} \frac{N}{\tau_n}. \quad (3)$$

J is the normalized pump current, which is determined by the injection current and the active volume of the laser; τ_n is the carrier lifetime; dg/dN is the differential gain; and N_{th} is the carrier density at threshold. Γ_{conf} is the confinement factor, which accounts for the fact that only a part of the optical mode is in the active volume. τ_s is the photon lifetime, and β is the fraction of the spontaneous emission that is coupled into the lasing mode.

The photon decay rate $1/\tau_s$ is separated into two terms, one describing the usual losses; the second, describing the additional losses that are due to the AR coating. In particular, we set

$$\frac{1}{\tau_s} = v_g \{ \alpha_{int} - \ln[R_1 R_2 (1 - r_2)] / 2L \}, \quad (4)$$

with the group velocity v_g , the internal losses α_{int} , the original reflectivities R_1 and R_2 of the LD facets, and the diode length L . The term $1 - r_2$ describes the decrease of the facet reflectivity caused by the AR coating. This equation can be written as

$$\frac{1}{\tau_s} = \Gamma + \kappa, \quad (5)$$

where Γ is the modified photon decay rate without coating and $\kappa = v_g [-\ln(1 - r_2) / 2L]$ is the variation of the photon decay rate that is due to the coating. With this Ansatz, we obtain a simple expression for the threshold current density J_{th} as a function of the coating-induced losses κ :

$$J_{th} = \frac{N_{th}}{\tau_n} + \frac{\kappa}{\tau_n G_N}, \quad (6)$$

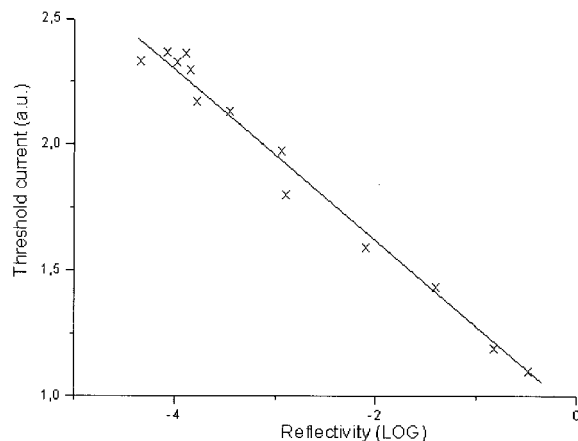


Fig. 4. Normalized threshold current as a function of the facet reflectivity in a semilogarithmic plot. Some of the measured threshold shifts for the AR-coated GaN laser diodes are shown as crosses in the graph.

where τ_n is the carrier lifetime and G_N is the differential gain. The threshold current linearly increases with κ . Inserting the expression for κ , one obtains the dependence of the threshold current density J_{th} as a function of the reflectivity. As schematically shown in Fig. 4, the threshold current density (normalized to its original value) exhibits an exponential dependence on the reflectivity.

C. Tuning Enhancement Effect, Part I

AR coatings strongly enhance the total tuning range of LDs. The origin of this positive effect can be explained in terms of the band structure $E(k)$ of the semiconductor material. As described by the equilibrium solution of Eq. (2), increasing the injection current of a LD causes an increase of the number of injected electrons and holes into the active area of the LD. Below threshold, this causes an increase of the carrier density N within the active region. Above threshold, the carrier density N remains constant, and the increase of the injection current only causes an increase of the optical power, which is proportional to an increase of the injection current. This effect is known as gain saturation.

One of the most obvious effects of AR coatings on LDs is the shift of the threshold current to higher current values as described above. This results in a larger carrier density N at the threshold for AR-coated LDs compared with uncoated LDs. LDs are nonequilibrium semiconductor devices. Formally, this is described by a splitting of the Fermi level into quasi-Fermi levels that describe the distribution of electrons and holes individually.¹⁹ Figure 5 shows the well-known band structure of a direct semiconductor in this case. Higher values of the carrier density cause an increase of the energy splitting of the quasi-Fermi levels ΔE , which results in a violet shift of the spontaneous-emission spectrum of a LD with increasing injection current.

The tunability of AR-coated LDs with an external cavity in Littrow and in Littman configurations ben-

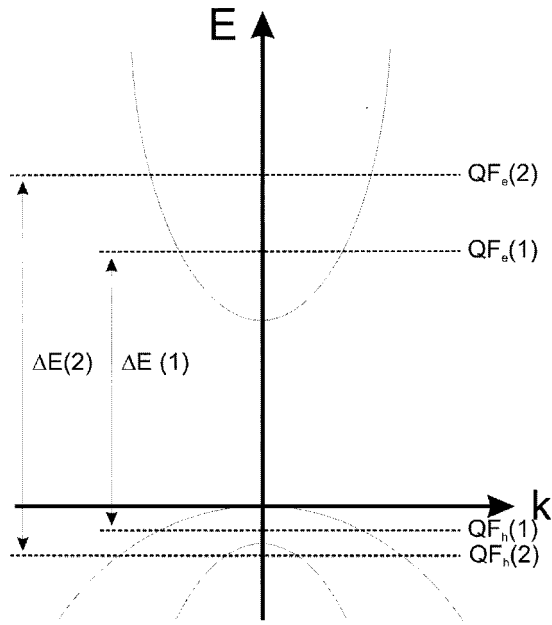


Fig. 5. Band structure of a direct semiconductor in a nonequilibrium case. The Fermi level splits up into a quasi-Fermi level for electrons (QF_e) and a quasi-Fermi level for holes (QF_h). The spectral maximum of the luminescence of the semiconductor material is defined by the energy difference ΔE between QF_e and QF_h . A higher value of the carrier density causes a higher value of the energy splitting ΔE , and the luminescence shows a violet shift.

efits from the described violet shift of the spontaneous emission. In particular, the tuning range is enlarged at the low-wavelength side of the total tuning range in comparison with a non-AR-coated diode laser in external cavity. The tuning enhancement effect can be clearly seen by comparison of the total tuning range of 6.3 nm for AR-coated blue diode lasers¹⁵ with non-AR-coated blue diode lasers.²⁰

D. Tuning Enhancement Effect, Part 2

AR coating strongly enhances the mode-hop-free tuning range of LDs in an external cavity. This effect can be explained within an analysis that has been performed for discussing the coherence collapse of diode lasers. Laser diodes with an external cavity show a sudden rise in the linewidth from a few hundred kilohertz up to several gigahertz depending on the feedback conditions.¹⁸ The dependence of the linewidth of such a laser system has been explained as a function of the feedback phase of the distant reflector,²¹ e.g., a grating. In particular, the region of line narrowing is closely located around the internal cavity mode of the diode laser. Outside this area the system may operate unstably and shows irregular modehops or multimode behavior.^{22,23} This is one reason for the limited tuning range that has been found for ECDL systems with non-AR-coated diode lasers.^{8,20,24} With AR coatings, mode-hop-free tuning ranges of more than 80 nm can be reached for 1550-nm ECDL systems.²⁵

The Littman configuration worked only with AR-coated diodes, whereas we also get a non-AR-coated

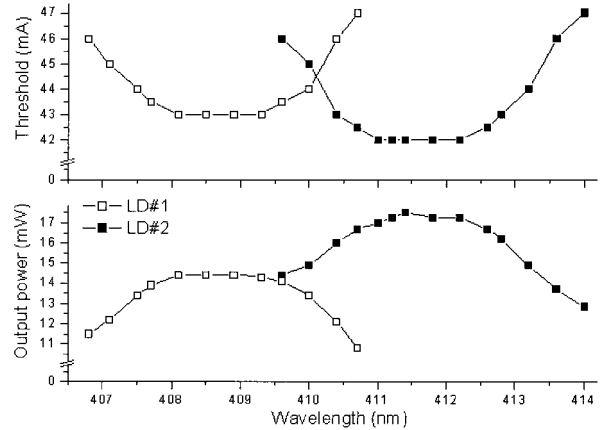


Fig. 6. Threshold current versus output wavelength (top) and optical output power versus wavelength (bottom), respectively, of two exemplary GaN LDs in Littrow configuration.

blue LD to work in a Littrow cavity with high feedback from a grating, resulting in lower power. However, the system was very hard to align, was unstable, and proved difficult to use, even for a trained operator. In our opinion, such a laser still needs further development in order to fulfill the requirements for high-precision experiments. Section 3 shows the excellent performance of the AR-coated blue diodes achieved with our Littrow cavity.

3. Characterization of the Littrow External Cavity Diode Laser

Two AR-coated LDs (#1 and #2) emitting at approximately 410 nm were exemplarily implemented in a Littrow cavity.⁹ The upper part of Fig. 6 shows the threshold current versus wavelength of the two EC-DLs. The threshold current follows the characteristic gain profile of the LD. The total tuning range of the LD in the external cavity at room temperature is shown in the lower part of Fig. 6. For LD#1 a total tuning range of 3.9 nm from 406.8 to 410.7 nm was observed at 21 °C. LD#2 was also tuned by 3.9 nm from 409.9 to 413.8 nm at 21 °C. In general, the wavelength of LD emission can be tuned by temperature.⁴ LD#2 in the cavity can be tuned by means of tilting the grating down to 409.7 nm at a temperature of 17 °C and up to 414.0 nm at 25 °C. These wavelength limits are also indicated in Fig. 6. The wavelength shift (achieved with tilting the grating) resulting from LD temperature is approximately ± 0.05 nm/K. The maximum optical output power was 14.4 mW for LD#1 and 17.2 mW for LD#2, both at 60-mA operation current. For obtaining such high output power, a grating with an efficiency below 20% with 3600 lines mm^{-1} was employed according to Eq. (1). The total tuning range could be increased up to 6.3 nm by use of a higher efficiency grating,¹⁵ accompanied by a decrease of the output power resulting from the described tuning enhancement effect of the AR coatings.

At the gain maximum the dependence of the output power on the diode current was detected for LD#2.

Before coating and without external cavity, the threshold current for LD#2 was at 31 mA and the slope efficiency after threshold was 0.83 W/A with a maximum available output power of 5 mA. These values are in agreement with specifications given by the Nichia Corporation.⁶ After AR coating and without external cavity, the threshold current was 47 mA and an output power of 22.4 mW at 64 mA operation current was measured (slope efficiency after threshold of 0.92 W/A). However, without the resonator, multimode emission was observed. For LD#2 in the Littrow cavity, the threshold was 43 mA and the slope efficiency after threshold was 0.88 W/A with an output power of 19.8 mW at 64-mA operation current. To describe a LD with an external cavity, Eq. (3) needs to include one additional term for describing the feedback from the distant reflector. This additional term on the right-hand side of Eq. (3) reads as

$$+\kappa_f S(t - \tau), \quad (7)$$

which describes the light coupled back from the external cavity. κ_f describes the feedback rate from the distant reflector. The feedback rate κ_f can be written in terms of the mirror reflectivity of the laser facet and of the distant reflector. $S(t - \tau)$ describes the photon density that is fed back into the laser chip. The delay term $(t - \tau)$ acknowledges the time delay of the laser light resulting from the roundtrip time τ of the external cavity. The steady-state solution of Eqs. (2) and (3) reads for these conditions as

$$N = N_{th} - \frac{2\kappa_f}{G_N}, \quad (8)$$

$$S = \frac{J - \gamma N}{\Gamma - 2\kappa_f}. \quad (9)$$

Equation (8) describes the feedback effect on the carrier density N of the diode laser. One clearly can read the threshold-lowering effect on external feedback from this description, which is in excellent agreement with the experimental results shown in Fig. 7.

Equation (9) describes the feedback effect on photon density S within the laser chip. To get an expression for the output power in milliwatts, one needs to take into account the output probability of the laser facet including the output directioning according to Eq. (1). In Fig. 7, the PI curve of the AR-coated LD without external cavity and the PI curve of the same AR-coated LD with external cavity feedback show a crossover at ~ 57 mA.

These effects can be understood according to Eq. (1). Increasing the reflectivity of laser facet R_1 induces a reduction of the power I_1 emitted from this laser facet. The power I_2 from the opposite laser facet with the unchanged facet reflectivity R_2 increases. Because of the additional reflectivity of the grating of the external cavity, the effective reflectivity of the external cavity side of the laser chip is in-

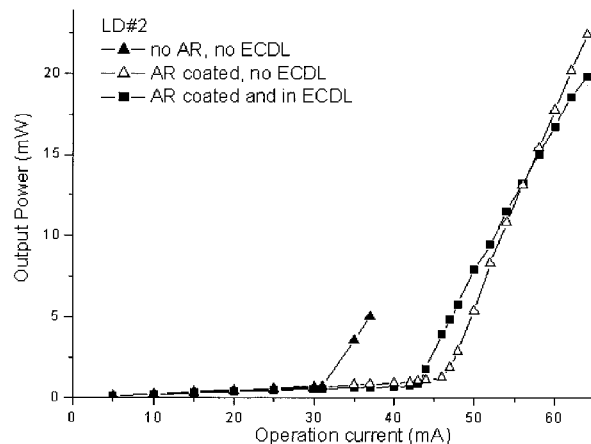


Fig. 7. Different PI curves of LD#2: first, without AR-coating and without external cavity; second, with AR-coating but still without resonator; and third, with AR coating and in Littrow resonator.

creased, and therefore the fraction I_1/I_2 of the light that is emitted from the external cavity side of the diode laser is reduced. As a result, we find the crossover as seen in Fig. 7.

This directioning effect of ECDL has an important practical relevance. For a large parameter range of ECDL, we can conclude the following: The lower the grating reflectivity that is chosen, the higher the output power of the ECDL coupled out by way of the cavity grating.

The (maximum) total output power of LD#1 in our Littrow cavity was 15.5 mW. Since LD#1 without AR coating already had a lower slope efficiency than LD#2 as specified by the Nichia Corporation,⁶ we expected a lower output power even in ECDL operation after AR coating. The ECDL shows excellent side-mode suppression as seen in Fig. 8. We have indicated the first side mode, which we have used for determining the side-mode suppression rate of 35 dB. Because of the AR coating, the side-mode suppression remains unchanged during wavelength scans. For another LD emitting at 405 nm in an external Littrow cavity, more than 30 mW in a single mode was

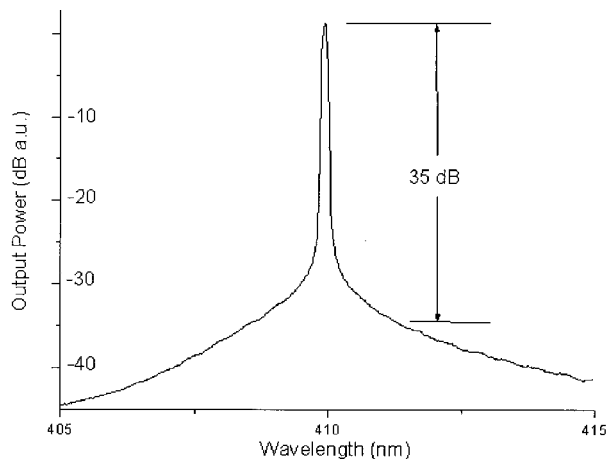


Fig. 8. Side-mode suppression of the ECDL at 410 nm.

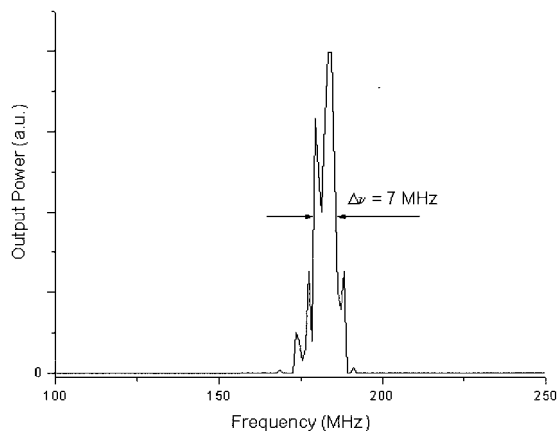


Fig. 9. Typical beat signal between two identical ECDLs at 410 nm (sweep time, 20 s).

observed. However, to ensure long lifetime we did not exceed 60-mA diode current. The output beam profile of the ECDL was $\sim 1:3$ elliptical with minor fringes at the sides of the beam, resulting from the diffraction at the collimator lens.

The linewidth of the ECDL was determined in a heterodyne experiment between two identical laser systems with superposed beams running at nearly the same wavelength. The beat signal was obtained with a fast photodiode. The indium absorption transitions described in Section 4 were used as a wavelength reference. The resulting beat signal was displayed and analyzed on a radio-frequency spectrum analyzer. The difference frequency was chosen to be in the range of between 100 and 600 MHz.

The linewidth of an ECDL is mainly determined by three factors. The first factor originates from acoustic disturbances and vibrations of the cavity. A typical frequency scale for these contributions to the linewidth is of the order of 1 kHz. To characterize this part of the linewidth, the first beat signal measurement was performed with a sweep time of 20 s. This long-term linewidth is 7 MHz for each ECDL as pictured in Fig. 9. The second factor is correlated to the shot noise of the injection current, which contributes to the linewidth at a frequency scale of approximately 1–10 MHz. The sweep time was 50 ms in this case, which results in a short-term linewidth of 0.8 MHz for each ECDL as depicted in Fig. 10. The third contribution is caused by relaxation oscillations that originate from the spontaneous-emission noise.^{26,27} A typical frequency scale is of the order of 1 GHz, which was not investigated in the present study. These results are consistent with previous results obtained for our near-infrared ECDL systems.⁹ The better performance observed with our ECDL systems compared with previously described ECDL²⁰ can be attributed to the good noise performance of our driver electronics. We have analyzed the tuning behavior of our ECDL system with a Fabry–Perot interferometer. Figure 11 shows a typical Fabry–Perot spectrum with a free spectral range of 8 GHz. We have found a mode-hop-free tuning

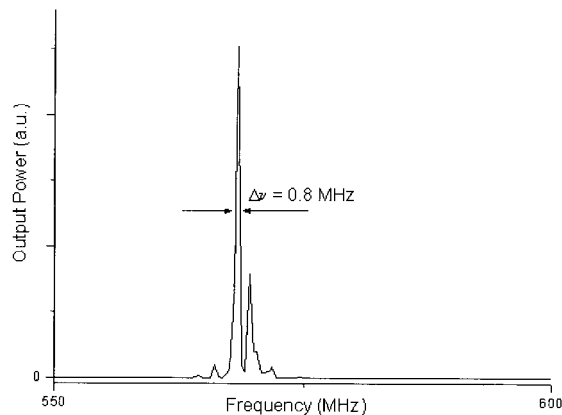


Fig. 10. Typical beat signal between two identical ECDLs at 410 nm (sweep time, 50 ms).

range of more than 50 GHz with our blue Littrow laser systems while benefiting from the current compensation technique. The current compensation technique involves an injection-current modulation simultaneous with the modulation of the piezovoltage for tuning the diffraction grating of the Littrow cavity.^{4,8,9,20} The linewidth and tuning behavior of the ECDL is sufficient for spectroscopic experiments with sub-Doppler resolution described in Section 4.

4. Doppler-Free Absorption Spectroscopy of Atomic Indium

Atomic indium has a $5^2P_{1/2}$ ground and a $5^2P_{3/2}$ and $6^2S_{1/2}$ excited state. Transitions between the $5^2P_{1/2}$ and $6^2S_{1/2}$ states are associated with absorption or emission of light with wavelengths around 410 nm, respectively. Transitions originating from the $6^2S_{1/2}$ excited state may also result in population of the $5^2P_{3/2}$ state accompanied by emission at 451 nm. The important isotopes are ^{115}In (95.7% natural abundance) and ^{113}In (4.3% natural abundance). They are characterized by a hyperfine splitting of 11.4 GHz in the ground state and 8.4 GHz in the $6^2S_{1/2}$ excited state. All excitation features are thus

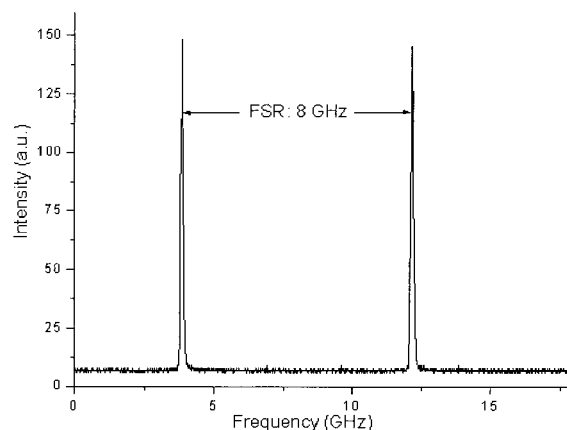


Fig. 11. Fabry–Perot spectrum of a blue GaN Littrow laser. The free spectral range of the scanning Fabry–Perot interferometer is 8 GHz as indicated by the arrow.

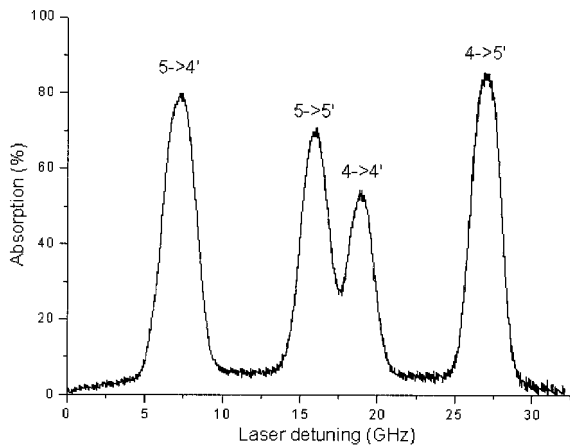


Fig. 12. Absorption features of indium vapor near 410 nm.

asymmetric doublets. Because the isotopic shift of 258.2 MHz is much smaller than the Doppler broadening (~ 2.5 GHz), individual ^{113}In and ^{115}In absorption features were not resolved with our setup. However, Leinen *et al.* have obtained detailed measurements of an indium atom beam.²⁰

In our experimental setup a beam splitter divided the laser beam in a strong pump and a weak probe beam passing approximately collinearly with opposite propagation directions through an indium cell. The cell was evacuated and heated to ~ 1300 °C to increase indium vapor pressure. The optical laser frequency was tuned by ~ 35 GHz without modehops—employing the current compensation technique previously described—over the absorption features of the indium vapor. The current compensation method is a procedure to increase the mode-hop-free tuning range but also results in a decrease of the output power. However, the measured spectra were corrected for these power variations. While the laser wavelength is tuned over a Doppler-broadened atomic absorption feature, all transitions of atoms belonging to velocity classes with velocity components in the laser propagation direction are excited and contribute to the linewidth of the observed absorption feature. With the pump beam blocked, the four Doppler-broadened absorption features were easily resolved (Fig. 12). All four hyperfine components for transitions from $F = 4, 5$ to $F' = 4, 5$ are resolved within one mode-hop-free scan. F is the hyperfine nuclear spin quantum number of the $5^2P_{1/2}$ ground state, and F' that of the $6^2S_{1/2}$ excited state. The hyperfine splitting of the absorption features observed were in good agreement with the hyperfine splitting of the fluorescence lines of the indium atom beam measured by Leinen *et al.*²⁰

Pump and probe beams are counterpropagating, and the only velocity class of atoms that is able to absorb the pump and the probe beam at the same time has a zero velocity component in the propagation direction of the laser beams. These transitions are saturated by the pump beam and should appear in the spectrum recorded with the probe beam as

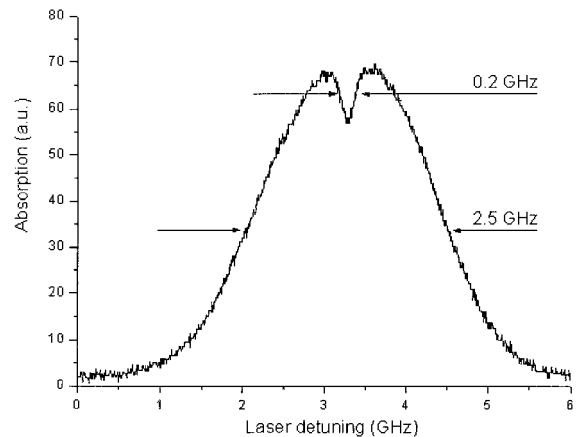


Fig. 13. Absorption feature of the $F = 5 \rightarrow F' = 4$ transition of indium vapor with the Lamb dip as observed with the saturated absorption experiment.

Lamb dips²⁸ in the profile of the Doppler-broadened absorption feature. The $F = 5 \rightarrow F' = 4$ transition absorption peak with a Lamb dip is shown in Fig. 13. The Doppler-broadened linewidth (FWHM) was measured as 2.5 GHz, whereas the linewidth of the Lamb dip was ~ 200 MHz. This measured linewidth of the Lamb dip is not determined by the natural linewidth of the transition, which is of the order of 25 MHz.²⁰ We can exclude a contribution from the linewidth of the laser source to the measured linewidth of the Lamb dip, since the linewidth of the ECDL is of the order of 1 MHz. On reason for the enlargement of the measured linewidth is that the spectral resolution of our experiment was determined by the crossing angle between the pump beam and the probe beam. This minor drawback of our results seems to be acceptable, since we have been using a simple, low-cost experimental setup with an indium vapor cell instead of an indium atomic beam.²⁰ Figure 14 shows a photograph of the indium cell that we have been using for our experiments, indicating the strong fluorescence stimulated by the laser. The method employed in this study is the classical saturated absorption experiment applied, e.g., for rubidium or cesium.^{29–32} Research in our facilities is in progress with an improved experimental setup utilizing a balanced receiver and a modified cell to achieve a better resolution of the Lamb dips.

5. Conclusions

The performance characteristics of an AR-coated GaN-based laser during operation in our Littrow external cavity lasers were investigated. The total tuning range was ~ 4 nm for each diode with optical output power of up to 30 mW. The obtained linewidth was 0.8 MHz with a mode-hop-free tuning of more than 50 GHz. The indium absorption spectrum near 410 nm with Lamb dips in the Doppler-broadened absorption features was detected by us of a standard saturated absorption setup. The linewidth and tuning behavior observed was in good agreement with results obtained previously for visi-

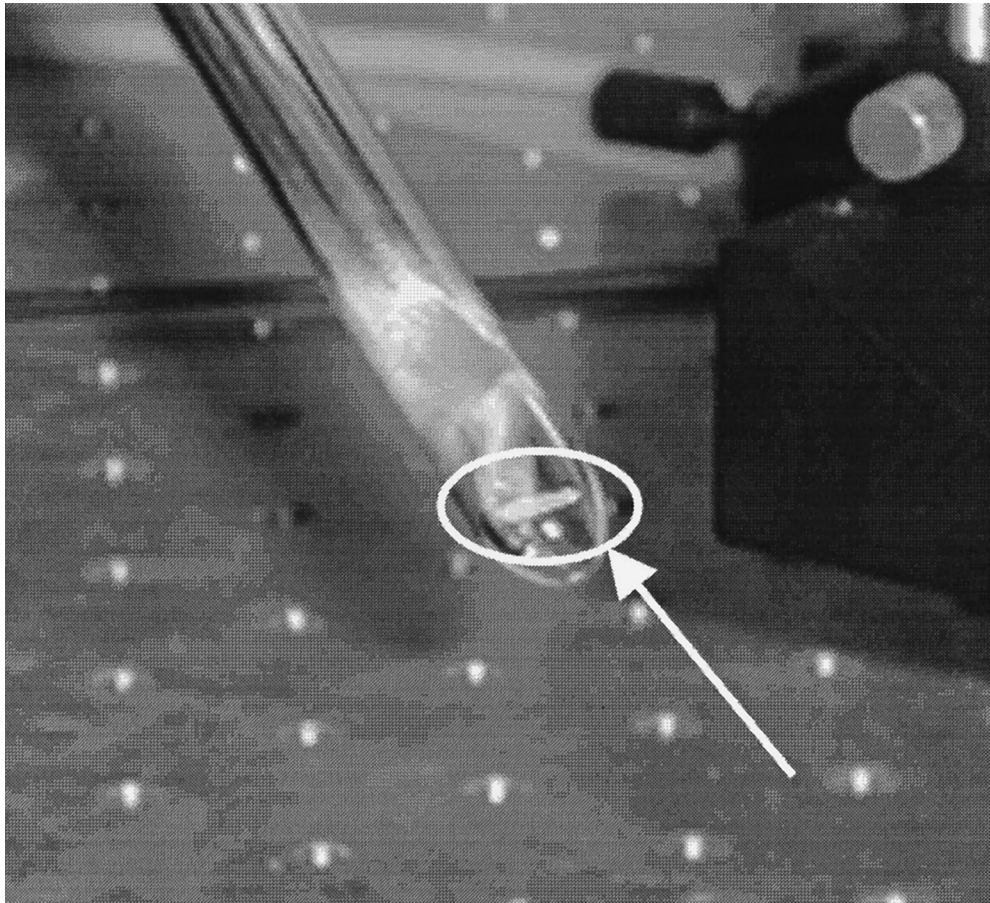


Fig. 14. Photograph of our indium cell indicating the fluorescence.

ble and near-infrared external cavity diode lasers. Although the actual width of the Lamb dips could not be satisfactorily resolved with the experimental setup we used, the appropriateness of the laser system for spectroscopic studies was emphasized.

References

1. R. N. Hall, G. E. Fenner, J. D. Kingsley, T. J. Soltys, and R. O. Carlson, "Coherent light emission from GaAs Junctions," *Phys. Rev. Lett.* **9**, 366–368 (1962).
2. M. I. Nathan, W. P. Dumke, G. Burns, F. H. Dill, Jr., and G. J. Lasher, "Stimulated emission of radiation from GaAs p-junctions," *Appl. Phys. Lett.* **1**, 62 (1962).
3. T. M. Quist, R. H. Rediker, R. J. Keyes, W. E. Krag, B. Lax, A. L. McWhorter, and H. J. Zeigler, "Semiconductor maser of GaAs," *Appl. Phys. Lett.* **1**, 91–92 (1962).
4. C. E. Wieman and L. Hollberg, "Using diode lasers for atomic physics," *Rev. Sci. Instrum.* **62**, 1–20 (1991).
5. S. Nakamura, S. Pearton, and G. Fasol, "The blue laser diode—the complete story," 2nd ed. (Springer, Berlin, 2000).
6. See <http://www.nichia.co.jp>.
7. J. W. Crowe and R. M. Craig, Jr., "GaAs laser linewidth measurements by heterodyne detection," *Appl. Phys. Lett.* **5**, 72–73 (1964).
8. L. Ricci, M. Weidemuller, T. Esslinger, A. Hemmerich, C. Zimmermann, V. Vuletic, W. Koenig, and T. W. Haensch, "A compact grating-stabilized diode laser system for atomic physics," *Opt. Commun.* **117**, 541–549 (1995).
9. See <http://www.sacher-laser.com>.
10. M. G. Littman and H. J. Metcalf, "Spectrally narrow pulsed dye laser without beam expander," *Appl. Opt.* **17**, 2224–2227 (1978).
11. J. Struckmeyer, A. Euteneuer, B. Smarsly, M. Breede, M. Born, M. Hofmann, L. Hildebrandt, and J. Sacher, "Electronically tunable external-cavity laser diode," *Opt. Lett.* **24**, 1573–1574 (1999).
12. M. Laschek, M. Reich, D. Wandt, W. Arens, C. Fallnich, and H. Welling, "External cavity diode laser with electrooptic wavelength tuning," in *Conference on Lasers and Electro-Optics*, OSA Technical Digest (Optical Society of America, Washington D.C., 1999), pp. 141–142.
13. D. Wandt, C. Fallnich, and H. Welling, "Laserdioden mit externen Resonatoren fuer die Gasanalyse," *tm-Technisches Messen* **68**, 365–373 (2001).
14. L. Hildebrandt, R. Knispel, and J. Sacher, "Kompakte External Cavity Dioden Laser fuer die industrielle Messtechnik," *tm-Technisches Messen* **68**, 374–379 (2001).
15. D. J. Lonsdale, A. P. Willis, and T. A. King, "Extended tuning and single-mode operation of an anti-reflection-coated InGaN violet laser diode in a Littrow cavity," *Meas. Sci. Technol.* **13**, 488–493 (2002).
16. J. Sacher, "Coating process and apparatus," U.S. patent 6,297,066 (2 October 2001).
17. I. P. Kaminow, G. Eisenstein, and L. W. Stulz, "Measurement of the modal reflectivity of an antireflection coating on a superluminescent diode," *IEEE J. Quantum Electron.* **QE-19**, 493–495 (1983).
18. J. Sacher, D. Baums, P. Panknin, W. Elsaesser, and E. O. Goebel, "Intensity instabilities of semiconductor lasers under

- current modulation, external light injection, and delayed feedback," *Phys. Rev. A* **45**, 1893–1905 (1992).
19. W. W. Chow, S. Koch, and M. Sargent III, *Semiconductor-Laser Physics* (Springer, Berlin, 1994).
 20. H. Leinen, D. Glaessner, H. Metcalf, R. Wynands, D. Haubrich, and D. Meschede, "GaN blue diode laser: a spectroscopist's view," *Appl. Phys. B* **70**, 567–571 (2000).
 21. G. P. Agrawal, "Line narrowing in a single-mode injection laser due to external optical feedback," *IEEE J. Quantum Electron.* **QE-20**, 468–471 (1984).
 22. P. Glas, A. Klehr, and R. Mueller, "Transient and stationary properties in bistable operation of a GaAs laser coupled to an external resonator," *Opt. Commun.* **44**, 196–200 (1983).
 23. J. Mork, B. Tromborg, and J. Mark, "Chaos in semiconductor lasers with optical feedback: theory and experiment," *IEEE J. Quantum Electron.* **QE-28**, 93–108 (1992).
 24. L. Hildebrandt and J. Sacher, "A comparison of AR-coated diode lasers and non AR-coated diode lasers, both within an identical external cavity," <http://data.sacher.de/arc/arbeneft.pdf>.
 25. F. Favre and D. Le Guen, "82 nm of continuous tunability for an external cavity semiconductor laser," *Electron. Lett.* **27**, 183–184 (1991).
 26. C. H. Henry, "Theory of the linewidth of semiconductor laser," *IEEE J. Quantum Electron.* **QE-18**, 259–264 (1982).
 27. C. H. Henry, "Theory of the phase noise and power spectrum of a single mode injection laser," *IEEE J. Quantum Electron.* **QE-19**, 1391–1397 (1983).
 28. W. Demtroeder, *Laser Spectroscopy*, 2nd ed. (Springer, Berlin, 1998).
 29. U. Tanaka and T. Yabuzaki, "Frequency stabilisation of diode laser using external cavity and Doppler-free atomic spectra," *Jpn. J. Appl. Phys.* **33**, 1614–1622 (1994).
 30. A. M. Akulshin, V. A. Sautenkov, V. L. Velchansky, A. S. Zibrov, and M. V. Zverkov, "Power broadening of saturation absorption resonance on the D₂ line of rubidium," *Opt. Commun.* **77**, 295–298 (1990).
 31. S. Nakayama, "Theoretical analysis of Rb and Cs D₂ lines in Doppler-free spectroscopic techniques with optical pumping," *Jpn. J. Appl. Phys.* **24**, 1–7 (1985).
 32. K. B. MacAdam, A. Steinbach, and C. Wieman, "A narrow-band tunable diode laser system with grating feedback, and a saturated absorption spectrometer for Cs and Rb," *Am. J. Phys.* **60**, 1098–1111 (1992).